






Geophysical Research Letters



RESEARCH LETTER

10.1029/2020GL091805

Climate Impacts of COVID-19 Induced Emission Changes

A. Gettelman^{1,2} , R. Lamboll³ , C. G. Bardeen¹ , P. M. Forster⁴ , and D. Watson-Parris² 

Key Points:

- COVID-19 induced lockdowns significantly altered emissions of aerosols, leading to simulated changes in cloud properties in two Earth System Models
- Aerosol Cloud Interactions from reduced emissions result in significant increases in radiative forcing, up to $+0.29 \pm 0.15 \text{ Wm}^{-2}$
- Aerosol radiative forcing reductions are the largest contributor to surface temperature changes

Supporting Information:

- Supporting Information S1

Correspondence to:

A. Gettelman,
andrew@ucar.edu

Citation:

Gettelman, A., Lamboll, R., Bardeen, C. G., Forster, P. M., & Watson-Parris, D. (2021). Climate impacts of COVID-19 induced emission changes. *Geophysical Research Letters*, 48, e2020GL091805. <https://doi.org/10.1029/2020GL091805>

Received 23 NOV 2020

Accepted 21 DEC 2020

¹National Center for Atmospheric Research, Boulder, CO, USA, ²Atmospheric, Oceanic and Planetary Physics, Oxford University, Oxford, UK, ³Imperial College, London, UK, ⁴Priestly Centre, University of Leeds, Leeds, UK

Abstract The COVID-19 pandemic led to dramatic changes in economic activity in 2020. We use estimates of emission changes for 2020 in two Earth System Models (ESMs) to simulate the impacts of the COVID-19 economic changes. Ensembles of nudged simulations are used to separate small signals from meteorological variability. Reductions in aerosol and precursor emissions, chiefly black carbon and sulfate (SO_4), led to reductions in total anthropogenic aerosol cooling through aerosol-cloud interactions. The average overall Effective Radiative Forcing (ERF) peaks at $+0.29 \pm 0.15 \text{ Wm}^{-2}$ in spring 2020. Changes in cloud properties are smaller than observed changes during 2020. Impacts of these changes on regional land surface temperature range up to $+0.3 \text{ K}$. The peak impact of these aerosol changes on global surface temperature is very small ($+0.03 \text{ K}$). However, the aerosol changes are the largest contribution to radiative forcing and temperature changes as a result of COVID-19 affected emissions, larger than ozone, CO_2 and contrail effects.

Plain Language Summary The COVID-19 pandemic changed emissions of gases and particulates. These gases and particulates affect climate. In general, human emissions of particles cool the planet by scattering away sunlight in the clear sky and by making clouds brighter to reflect sunlight away from the earth. This paper focuses on understanding how changes to emissions of particulates (aerosols) affect climate. We use estimates of emissions changes for 2020 in two climate models to simulate the impacts of the COVID-19 induced emission changes. We tightly constrain the models by forcing the winds to match observed winds for 2020. COVID-19 induced lockdowns led to reductions in aerosol and precursor emissions, chiefly soot or black carbon and sulfate (SO_4). This is found to reduce the human caused aerosol cooling: creating a small net warming effect on the earth in spring 2020. Changes in cloud properties are smaller than observed changes during 2020. The impact of these changes on regional land surface temperature is small (maximum $+0.3 \text{ K}$). The impact of aerosol changes on global surface temperature is very small and lasts over several years. However, the aerosol changes are the largest contribution to COVID-19 affected emissions induced radiative forcing and temperature changes, larger than ozone, CO_2 and contrail effects.

1. Introduction

The COVID-19 pandemic resulted in “lockdowns” worldwide in the first half of 2020. These changes to the global economy and movement of people changed fossil fuel and transport use (IEA, 2020), altering CO_2 emissions, as well as emissions of aerosols and aerosol precursors (Le Quéré et al., 2020). Observations confirm that these changes had impacts on the atmosphere. There were regional changes in industrial emissions (Lian et al., 2020; R. Zhang et al., 2020) and pollutant levels dropped (Venter et al., 2020), even accounting for meteorology (Goldberg et al., 2020). Aerosol optical depth was reduced over China during February lockdowns (Diamond & Wood, 2020). Some regions, however, may have experienced more pollution (Le et al., 2020) due to complex chemical buffering (Sicard et al., 2020) and meteorology. The changes to fossil fuel use and transport impacted anthropogenic aerosols like black carbon (BC, colloquially “soot”) and sulfate (SO_4). Forster et al. (2020) extended emissions estimates from Le Quéré et al. (2020) using Google mobility data to generate a nearly worldwide data set of emissions reductions.

BC and SO_4 aerosols are important for climate (Bellouin et al., 2020), both for direct scattering (SO_4) and absorption (BC) of radiation, as well as for their indirect effect on clouds. Aerosols act as Cloud Condensation Nuclei (CCN) and are locations for nucleating liquid drops and ice crystals. Decreases in aerosols would

© 2020. The Authors.

This is an open access article under the terms of the [Creative Commons Attribution License](https://creativecommons.org/licenses/by/4.0/), which permits use, distribution and reproduction in any medium, provided the original work is properly cited.

tend to result in fewer cloud drops (Twomey, 1977), which would result in dimmer low clouds, and more absorption of radiation (warming). Decreases in drop numbers and increases in drop size further affect cloud microphysics, potentially increasing precipitation and altering cloud lifetime (Albrecht, 1989). Any reduction of anthropogenic aerosols would reverse their effect on cooling the planet from anthropogenic emissions over the industrial era (Bellouin et al., 2020). Yang et al. (2020) note simulated increases in surface temperature as a result of aerosol reductions. Diamond and Wood (2020) looked at initial results from early lockdowns in China on aerosols and found small and not very significant changes in cloud microphysics. Weber et al. (2020) also found limited effects of hypothesized changes in emissions with a chemical model.

In this study, we use estimates of emissions changes based on observations and focus particularly on Effective Radiative Forcing (ERF) due to aerosols: Direct Aerosol Radiation Interactions (ERF_{ARI}) and indirect Aerosol Cloud Interactions (ERF_{ACI}). To explore these questions, we use a constrained configuration of two Earth System Models focusing on the atmosphere, which can also tell us something about temperature changes, at least over land. We will not focus on air pollution chemistry (especially ozone) in urban regions, which has complex responses to emissions reductions (Sicard et al., 2020).

Our hypothesis is that we can use constrained models nudged to meteorology to reduce noise and get detectable signals. We further hypothesize that the signal will be small, or not significant in many (most) regions, and the magnitude of the physical signals can be compared to observations. This has implications for attribution of COVID-19 induced emission changes from observations. We hypothesize that the reduction of aerosols may be detectable, and may generate a positive ERF from reductions in aerosols. Depending on regime and location, this may affect surface temperature and temperature extremes in 2020, and even precipitation. The integrated effect of these ERF changes over time may also be detectable on surface temperature. The changes in GHG emissions (CO_2 , CH_4) are expected to be on the order of 20% (IEA, 2020), which is small on the short term ERF, but may be detectable on longer timescales. For a comparison of the impact between short and long term ERF we will use climate model emulator estimates to understand the impacts on ERF and surface temperature.

Methods are described in Section 2, Results are divided into specific effects of aerosols leading to changes in ERF (Section 3) and subsequent effects on climate (Section 4). Conclusions are in Section 5.

2. Methods

2.1. Models

We perform simulations with two different ESMs. One is the Community Earth System Model version 2 (CESM2), (Danabasoglu et al., 2020). The atmospheric model in CESM is the Community Atmosphere Model version 6 (CAM6), described by Gettelman et al. (2020). CAM6 features a detailed two-moment cloud microphysics scheme (Gettelman & Morrison, 2015) coupled to an aerosol microphysics and chemistry model (Liu et al., 2016), as detailed in Gettelman et al. (2019). We also perform simulations with the ECHAM6.3–HAM2.3 model (Neubauer et al., 2019), which couples the HAM aerosol module (Stier et al., 2005; K. Zhang et al., 2012) to the ECHAM6 atmospheric general circulation model (Stevens et al., 2013) and also uses a two-moment cloud microphysics scheme (Lohmann & Neubauer, 2018).

2.2. Simulation and Emissions

For CESM we use the standard resolution ($\sim 1^\circ$ horizontal resolution, 32 levels to 3 hPa), in a nudged configuration as described by Gettelman et al. (2020). The model time step is 1,800s. Winds, Sea Surface Temperatures (SST), and temperatures are relaxed to NASA Modern-Era Retrospective analysis for Research and Applications, version 2 (MERRA2) (Molod et al., 2015), available every 6 h. The system is run with specified (nudged SSTs), but an interactive land surface model (the Community Land Model version 5 in CESM2, Danabasoglu et al., 2020). Simulations are spun up for the year 2019, and then 20 ensemble members are launched from January 1, 2020 to August 31, 2020, with a small round off perturbation ($10^{-10}K$) to temperature. The perturbation generates a slightly different evolution of the atmosphere in each ensemble member. Nudging keeps the atmosphere in a similar state, but the perturbation samples the random noise within that

state, and enables estimates of the statistical significance of differences. Statistical significance is defined using the False Discovery Rate (FDR) method of Wilks (2006), which reduces patterned noise.

ECHAM-HAM simulations are run over the same period with $\sim 2^\circ$ horizontal resolution and 47 levels to 0.01 hPa. These simulations used climatological SSTs and are nudged to the ERA5 (Hersbach et al., 2020) meteorological winds, but not atmospheric temperatures. The same emissions scenario (from Forster et al., 2020) is run as for CESM using monthly emissions. An ensemble of 17 members is similarly created with small initial perturbations. The ECHAM-HAM simulation set up is most similar to the CESM “NoT” ensemble described below.

We use the Shared Socioeconomic Pathway (SSP) 245 as the “control” simulation without effects of emissions changes due to COVID-19. We then apply the 2020 sector activity estimates from the methods of Forster et al. (2020) to SSP2-4.5 gridded emissions data. Emissions data are available as monthly (<https://doi.org/10.5281/zenodo.3957826>) and daily (<https://doi.org/10.5281/zenodo.3952959>) averages. Daily averages are a running 7-day mean to remove any day-of-week effects. ECHAM-HAM and the CESM “COVID-19” scenario use monthly averages. We generate ensembles of simulations for both control and COVID-19 perturbations.

Several sets (ensembles) of simulations are run in CESM with the same nudging methodology to understand sensitivity to the methodological choices in setting up the simulations. The “COVID-19” ensemble uses monthly data and nudged winds and temperatures (the same as the ECHAM-HAM ensemble). Additionally, for CESM, we adjust the simulations with two sets of additional simulations (20 ensemble members for both the control and perturbation). The “NoT” ensembles (control and COVID-19 affected emissions) are run without nudging temperatures (but still nudging SST). The “NoT” ensembles enable an assessment of changes in vertical temperature structure and surface temperature over land, and are most similar to the ECHAM-HAM ensemble. We also perform a CESM ensemble with daily instead of monthly emissions (“Daily”). Since lockdowns were sudden and varied in different countries, as well as because meteorology might be correlated with emissions, this might yield different answers.

These simulations allow a fast temperature adjustment. The ECHAM-HAM and CESM “NoT” ensembles allow more freedom for temperature adjustment. The resulting perturbations in radiative fluxes are thus an Effective Radiative Forcing (ERF) and we will refer to them that way. Our goal is to define the ERF produced from the hypothesized emissions changes. Finally, we will use the FaIR model (Smith et al., 2018) as applied by Forster et al. (2020) to turn the monthly ERF into a hypothesized surface temperature change. This study differs from previous work by Yang et al. (2020) by using an updated modeling framework, with ensemble statistics, multiple ESMs and with a more extensive sampling period and emissions reductions, as well as a more comprehensive look at surface temperatures.

3. Results: Aerosol Effective Radiative Forcing

Figure 1 illustrates the March zonal mean perturbation in aerosols as a result of the COVID-19 lockdowns. March is chosen to highlight differences between daily and monthly averaged emissions. The shading shows the standard deviation of the ensemble members for each of four ensembles (three from CESM and one from ECHAM-HAM). The variability around the ensemble mean is much larger without temperature nudging, as expected. The changes in aerosol optical depth (Figure 1a) are significant (more than two standard deviations different from zero when temperatures are nudged), driven mostly by sulfate (Figure 1b) and black carbon (BC) changes (Figure 1c). ECHAM-HAM simulations (Figure 1, red line) have similar structure to CESM (compare to the NoT simulation, blue in Figure 1). ECHAM-HAM has higher AOD changes in the subtropics (Figure 1a), with similar change in BC burden (Figure 1c) and less difference in sulfate burden (Figure 1b). Differences result from reductions in Northern India and Eastern China (see Figures S1 and S2). The base state AOD in ECHAM is higher than CESM over China. So the same sulfur burden has a higher AOD, so the same change in emissions will result in a larger change in AOD. There are small but significant changes in some latitudes in clear-sky net shortwave fluxes in both models (Figure 1d) representing the direct effect of aerosols. These come from increases (warming) due to reductions in sulfate and cooling due to reductions in BC. There is little significant change in zonal mean shortwave Cloud Radiative

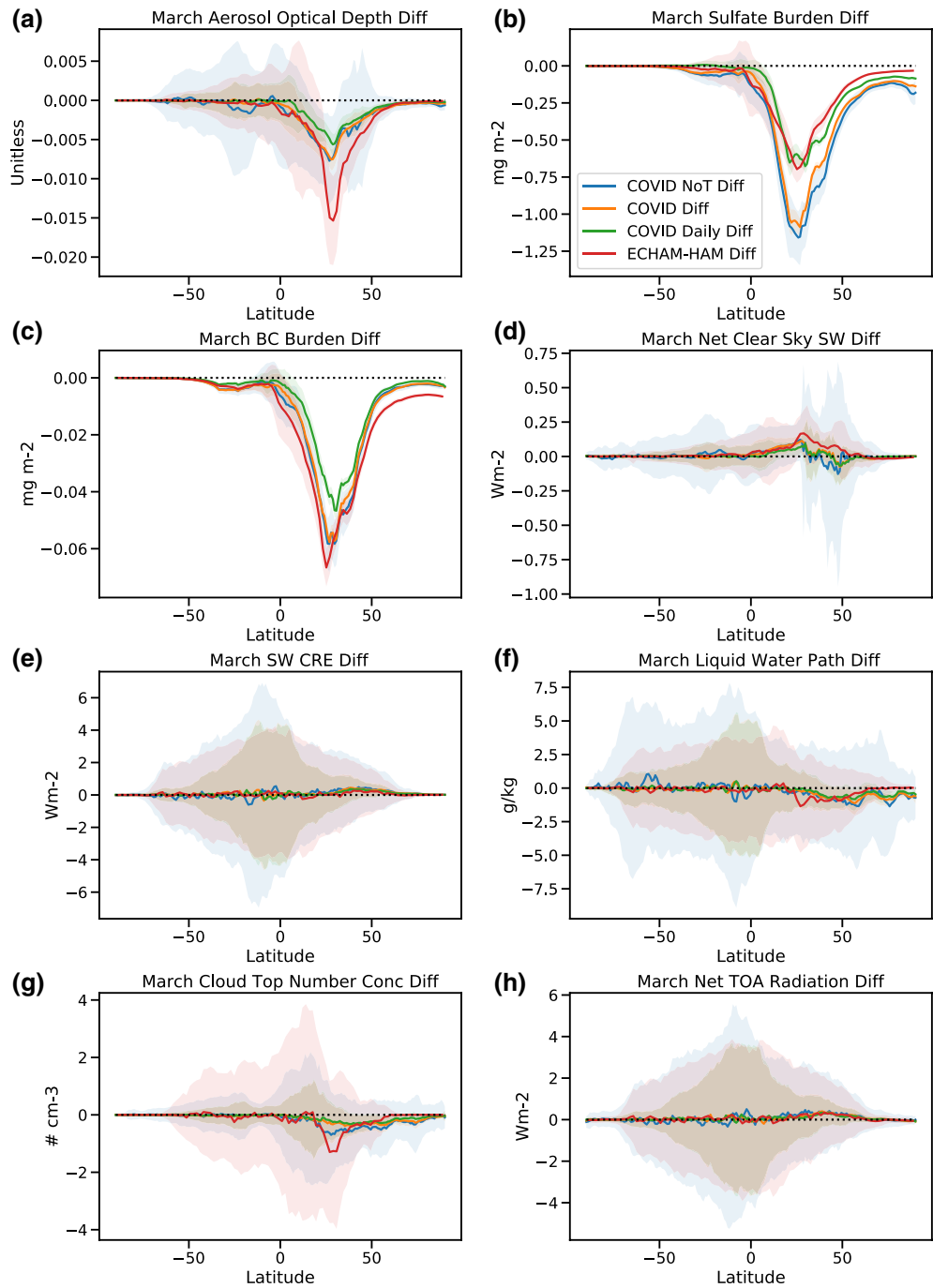


Figure 1. Zonal mean perturbations as a result of the COVID19 lockdowns averaged over March 2020. Shading shows the standard deviation of the ensemble members and solid line is the mean. CESM COVID-19 ensemble (COVID, orange), no temperature nudging (COVID NoT, blue), daily emissions with temperature nudging (COVID Daily, green) and ECHAM-HAM simulations without temperature nudging (ECHAM-HAM, red). (a) Aerosol optical depth, (b) total column sulfate (SO_4), (c) total column black carbon (BC), (d) clear-sky Net shortwave flux at TOA, (e) shortwave cloud radiative effect (CRE), (f) liquid water path (LWP), (g) cloud top number concentration, and (h) net TOA radiation difference. CESM, community earth system model; TOA, top of atmosphere.

Effects (SW CRE) in March (Figure 1e). Drop number (Figure 1g) and liquid water path (LWP) (Figure 1f) decreased in both models (Albrecht, 1989 and Twomey, 1977 effects). These effects lead to opposite changes in drop number that result in nearly constant drop size (not shown). The net effect results in small increases in Top Of Atmosphere (TOA) net radiation flux (Figure 1h). March is the month that the lockdowns began outside of China, and simulations with daily emissions (COVID Daily) show significant differences in sulfate and BC from the ensemble with monthly mean emissions since the changes happened toward the end of March 2020. Other months show little difference between daily and monthly emissions simulations.

Most lockdowns outside of China occurred between March and June 2020. Figure 2 shows the global monthly mean evolution of the quantities from Figure 1. Shading indicates one standard deviation of global means across each ensemble. Note that the ECHAM-HAM and CESM “NoT” ensembles have the highest variance because they do not nudge temperature. Figure 1 illustrates the increase in reductions until May, and then the beginning of a recovery in June 2020. ECHAM-HAM simulations were 7 months, CESM simulation 8 months. Daily emissions (Green) only differ substantially in March. The evolution of the fields is consistent with the zonal mean picture: reductions in aerosols (Figure 2a), driven by sulfate (Figure 2b) and BC (Figure 2c), yield an increase in clear-sky flux of up to 0.1 Wm^{-2} globally in May. Sulfate burden differences are lower in ECHAM-HAM, but most other quantities are consistent between models. Large ECHAM-HAM AOD variance in June 2020 is due to dust storms in some ensemble members. There are changes in SW Cloud Radiative Effect (Figure 2e) peaking in April and May, driven by decreases in LWP (Figure 2f), decreases in Cloud Drop number (Figure 2g) and resulting in a combined TOA flux averaged over April–June 2020 in the two ESMS without temperature nudging of $+0.29 \pm 0.15 \text{ Wm}^{-2}$ (Figure 2h). The uncertainty is 2 standard deviations around the ensemble mean for the ensembles without temperature nudging (Blue for CESM and Red for ECHAM in Figure 2). Figure 3a shows the pattern of TOA changes for May, which are significant only in isolated regions over land and ocean North of 45°N latitude in the CESM ensemble. ECHAM-HAM has a larger global mean perturbation to cloud drop number, consistent with Figure 1.

The spatial distribution and significance of these changes is illustrated in Figure S1 for CESM with temperature nudging and Figure S2 for ECHAM-HAM without temperature nudging. May is shown as the month of maximum difference. Aerosol changes are significant in most regions for both models, and clear-sky flux differences are significant over most of the Northern Hemisphere in both models. Liquid water path, cloud drop number and cloud forcing changes are significant over mid and high latitudes of the Northern Hemisphere in CESM, and there are also some significant differences over the S. Hemisphere subtropics and Mid-latitudes for liquid water path and cloud drop number when temperatures are nudged (Figure S1) in CESM. This likely results from changes in human and industrial emissions in the S. Hemisphere. TOA flux differences are significant over higher latitudes of the N. Hemisphere with temperature nudging, with lots of noise in the tropics. There is little TOA flux change in the S. Hemisphere, likely because of reduced solar insolation in May heading into S. Hemisphere winter. As expected, there is more significance to TOA fluxes in CESM with temperature nudging (Figure S1h) than without (Figure 3a).

How do these changes compare to satellite observations? Diamond and Wood (2020) attempted to estimate changes over China in February 2020 using observations, and found no significance for changes in AOD on the order of ± 0.2 and cloud drop radius changes of ± 2 microns. Figure S3 illustrates that simulated changes due to emissions would only be on the order of -0.05 AOD (significant) and $+0.1$ micron for effective radius (mostly not significant over China in February). Thus simulated changes of the magnitude found here cannot be ruled out by observations given the large year to year internal variability due to meteorology. Or stated another way, the differences due to COVID-19 induced emission changes are swamped by magnitude of interannual variability, and any year could easily have a difference from climatology larger than the signal due to emissions changes.

4. Results: Climate Impacts

Next we look at climate impacts of the emissions reductions. The reduction in aerosols causes a dimming of clouds and reduced clear-sky scattering, leading to a net absorption of radiation. This extends all the way to the surface. The short nudged simulations do not allow for a full climate response, but we can examine the

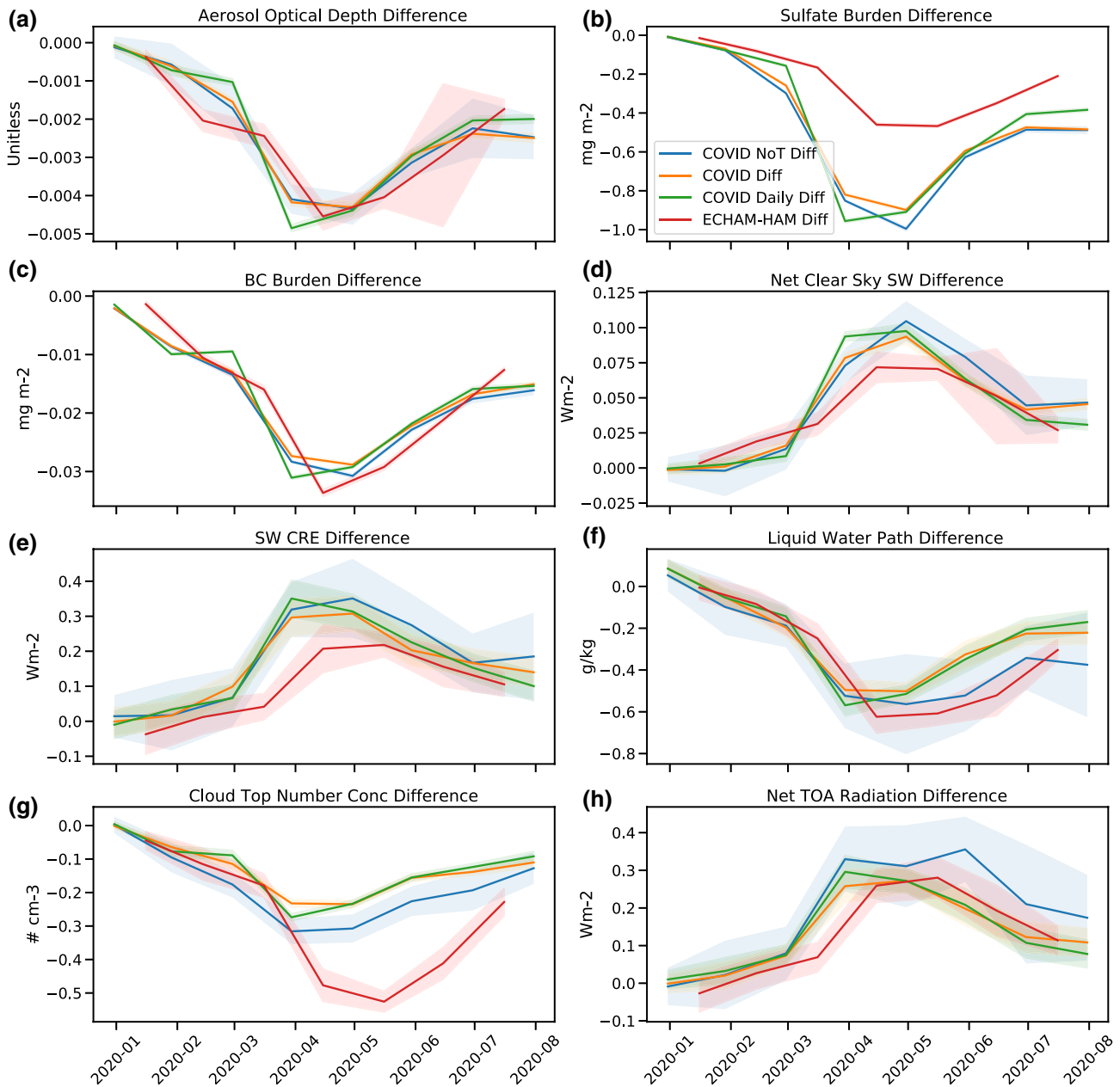


Figure 2. Monthly global mean time series of differences due to COVID-19 lockdowns. COVID-19 ensemble (COVID, orange), no temperature nudging (COVID NoT, blue), daily emissions with temperature nudging (COVID Daily, green) and ECHAM-HAM simulations (ECHAM-HAM, red). (a) aerosol optical depth, (b) total column sulfate (SO_4), (c) total column black carbon (BC), (d) clear-sky net SW flux at TOA, (e) SW cloud radiative effect (CRE), (f) liquid water path (LWP), (g) cloud top number concentration, and (h) net TOA radiation difference. Shading indicates one standard deviation of global means across the ensembles. SW, shortwave; TOA, top of atmosphere.

radiative impacts in the atmosphere and the land surface in simulations without temperature nudging. The ocean surface temperature is fixed, but the land surface, and surface temperature over sea ice will respond to radiative and surface fluxes.

Figure 3 shows surface climate differences resulting from the COVID-19 affected emissions changes in the ensembles without temperature changes for May, the month of peak radiative effect. Figures 3a and 3b are from the CESM NoT ensemble, while Figures 3c and 3d are from ECHAM-HAM (also without temperature nudging). Figures 3a and 3c show the net TOA radiative effect pattern, with moderate warming

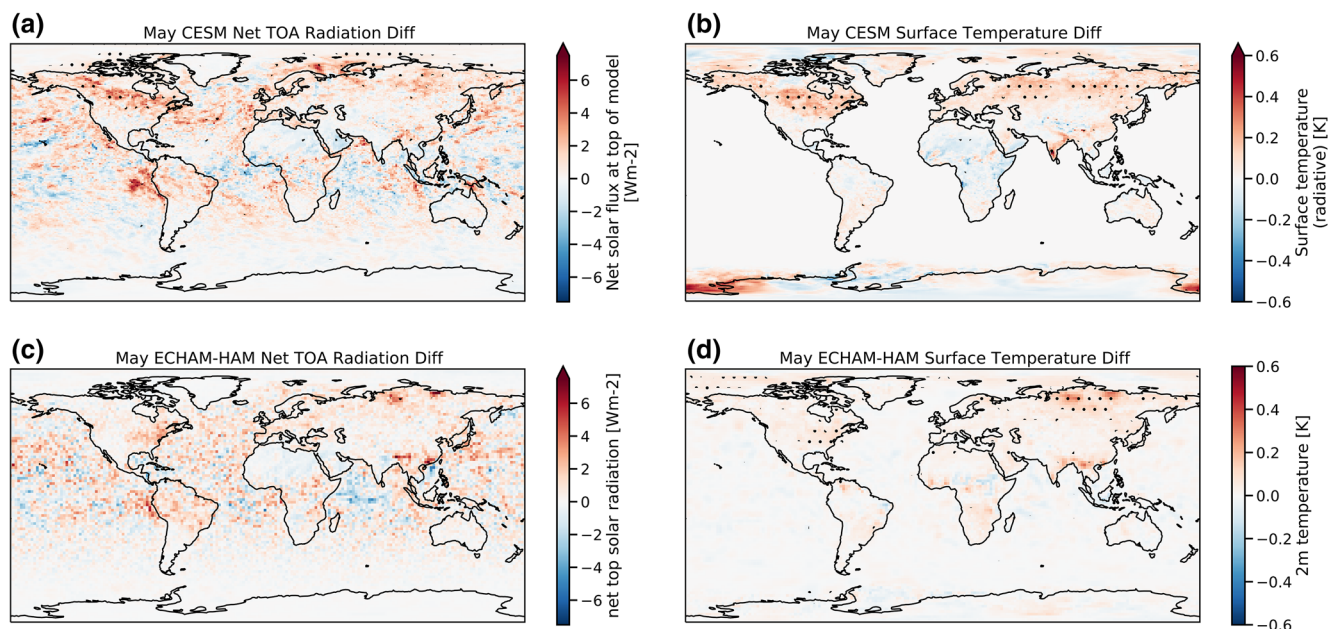


Figure 3. May 2020 simulated climate changes as the difference between COVID-19 and Control ensemble means without temperature nudging for (a), (c) net top of atmosphere Radiation, (b), (d) average surface temperature. (a), (b) CESM NoT ensemble (c), (d) ECHAM-HAM ensemble. Stippled regions are significant differences using an FDR test at 90% confidence. CESM, community earth system model; FDR, false discovery rate.

(not significant) over most N. Hemisphere land regions, and a noisy pattern in the tropics. Figures 3b and 3d show the mean surface temperature. Over the region from 45–60°N the average over land is 0.07 K, the average over the region of significant land warming is +0.13 K. It is largest over the US and Russia, where it reaches a maximum of +0.37 K in CESM (Figure 3c), slightly less in ECHAM-HAM (Figure 3d).

For CESM, we have also examined the minimum and maximum temperature over the month of May (defined as the highest and lowest temperature found that month) and found the differences (not shown) are very similar to the mean temperature change, indicating no substantially different changes in temperature extremes.

The vertical structure of temperature (Figure S4), illustrates that over most regions examined there is warming at the surface or in the lower troposphere, generally below clouds that reflect radiation, and cooling in the upper troposphere (~200 hPa). Temperature changes aloft are larger than those at the surface. The mid troposphere cools over India due to reductions in BC (Figure S1c) reducing absorption, while the reduction of scattering from sulfate and sulfate effects on clouds near the surface may be contributing to warming through more penetration of solar radiation to the surface. These changes do not seem to have significant effects on precipitation, either by the decrease in stability (which would perhaps increase regional precipitation) or through increases in the surface radiation (which could increase total regional surface fluxes and increase precipitation).

Simulations with fixed meteorology are not able to ascertain whether there would have been circulation effects due to the radiative changes. However, they are able to quantify an ERF (Figure 2h) and fast response surface temperature changes over land (Figures 3b and 3d) due to aerosol perturbations.

4.1. FaIR Model Temperature Effects

To understand the medium to long term effects of the temperature changes and the relative magnitude of the Aerosol ERF due to COVID-19 affected emissions changes, we use the FaIR climate model emulator version 1.5 (Smith et al., 2018), updating the aerosol ERF used in Forster et al. (2020). The FaIR model was set up to represent the response expected from the latest generation of climate models. The ERF for tropospheric ozone (O₃), CO₂ and contrails are taken from Forster et al. (2020) and the Aerosol ERF is updated

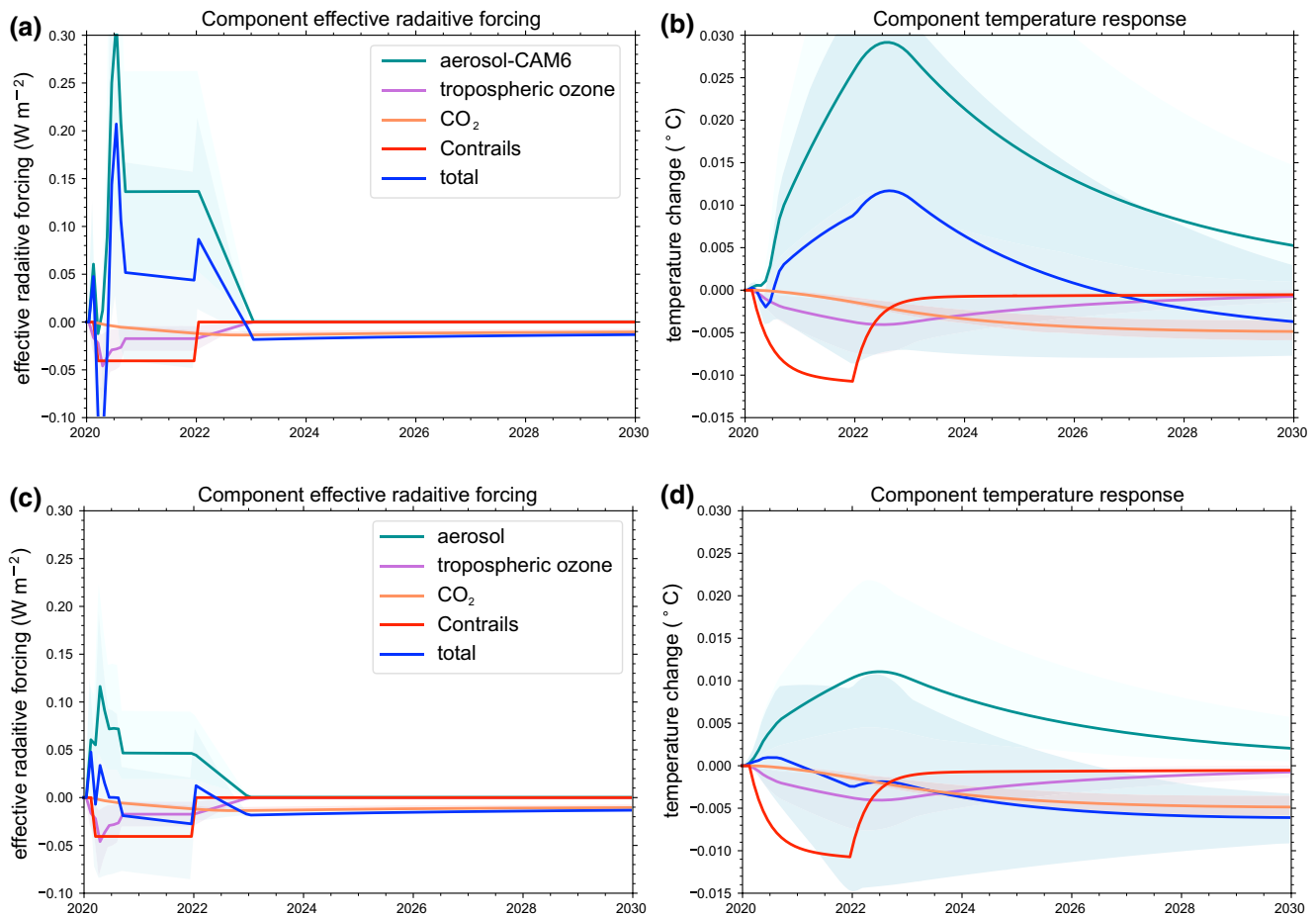


Figure 4. FaIR model estimates of (a), (c) Effective Radiative forcing and (b), (d) component temperature response for aerosols. Tropospheric ozone (purple), CO₂ (orange), Contrails (red) and Total (blue) from Forster et al. (2020). A,B use aerosol ERF from Figures 2c and 2d use the Aerosol ERF from Forster et al. (2020). O₃, CO₂ and contrails are updated from Forster et al. (2020). ERF, effective radiative forcing.

from this study using the CESM ERF as indicated in Figure 2h. Note that the O₃ ERF does not include detailed air pollution chemistry that could cause an increase in ozone locally (Le et al., 2020), so it should be regarded as the maximum ERF possible. After August the Aerosol ERF is reduced to 66% of the June value for two years and then ramps to 0 over 2022, assuming it takes a while for the world's emissions to return to normal. Given the similarity of the ECHAM-HAM ERF, we expect results to be very similar.

FaIR model simulations indicate that the aerosol ERF dominates over other COVID-19 ERF perturbations, and that this produces the largest temperature response, far outstripping cooling effects due to contrail, O₃ and CO₂ reductions. The CESM or ECHAM-HAM simulated aerosol ERF (Figure 2h) is larger than that assumed by Forster et al. (2020) (Figure 4c). The peak impact on global temperature would not be felt until 2022. The global estimate is quite small, but the regional temperature perturbations estimated here may be larger by a factor of 10 (Figure 3).

5. Discussion and Conclusions

In this work we have estimated the effects of COVID-19 affected emissions changes in 2020. We use two ESMs with similar complexity of their cloud and aerosol schemes, but very different implementations. The two models, CESM and ECHAM-HAM, yield very similar quantitative responses to the same emissions perturbations. The unique aspect of this study is we use simulations constrained by actual meteorology over 2020 to remove the effects of meteorological noise from the simulations. This results in the ability to find statistically significant changes much smaller than could be seen in observations (Diamond & Wood, 2020),

and differs in that regard from previous work. The limitation of the study is to use one set of emissions perturbation estimates from Forster et al. (2020), though that estimate has been compared to observations.

In CESM, we assess several different approaches to the simulations. We look at whether including daily varying emissions matters for a tighter correlation with meteorology. This only seems to matter in March 2020 when the largest gradients occur. We also looked at the impact of nudging or not nudging temperature. Nudging temperature reduces the variance across the ensemble, with little change in mean properties.

Significant changes in simulated aerosol emissions lead to reductions in total anthropogenic aerosol cooling through aerosol-cloud interactions in the simulations. Cloud drop numbers were reduced in the simulations and liquid water path decreases. This leads to a dimming of clouds and a net warming effect. The combined average ERF peaks at $+0.29 \pm 0.15 \text{ Wm}^{-2}$ in April–June 2020. The total anthropogenic ERF of these two models is on the higher end of estimates of Bellouin et al. (2020), on the order of -1.3 Wm^{-2} for ECHAM-HAM and -1.7 Wm^{-2} for CESM Gettelman et al. (2019). The 20% difference in total anthropogenic aerosol ERF is consistent with slightly smaller differences in ECHAM (Figure 2h).

The magnitude of these changes regionally significant in radiative and cloud properties only when tightly constrained simulations nudged to meteorology are used. The differences from baseline are much smaller than year to year variability in radiative and cloud properties due to meteorology, and thus not directly detectable from observations.

Though the simulations use fixed ocean temperatures, surface temperature over land can vary. Accordingly, the fast radiative response from clouds and aerosols does cause regional changes in surface temperature on the order of $+0.1$ to $+0.3 \text{ K}$, mostly at higher northern hemisphere latitudes. However, this result does not account for all the earth system dynamics or the slower response as the ocean interacts with radiation. To assess the longer term response but limit noise, we put the aerosol ERF derived here into the FaIR model estimates from Forster et al. (2020). The aerosol ERF estimates are larger than in Forster et al. (2020). The impact of these aerosol changes on global surface temperature is estimated to be very small ($+0.03 \text{ K}$ peak) and transient over several years. However, the aerosol changes are the largest contribution to COVID-19 affected emissions induced radiative forcing and temperature changes. Aerosol changes are larger than ozone, CO_2 and contrail cooling effects.

We have sampled uncertainty over climate noise with ensembles and with respect to different ESM formulations of aerosols and clouds. Forster et al. (2020) characterize their mobility based emissions changes as possibly representing an upper estimate, and we use of models with strong aerosol ERF, so the aerosol ERF here would be on the higher end of expectations. Further work should be done to extend these records and to sample uncertainties in emissions changes as more data become available.

Acknowledgments

The National Center for Atmospheric Research is supported by the United States National Science Foundation. CESM Simulations were performed at the NCAR Wyoming Supercomputing Center as part of the Climate Simulation Laboratory. Thanks to L. Emmons for processing the emissions data for CESM. The ECHAM-HAMMOZ model is developed by a consortium composed of ETH Zurich, Max Planck Institut für Meteorologie, Forschungszentrum Jülich, University of Oxford, the Finnish Meteorological Institute and the Leibniz Institute for Tropospheric Research, and managed by the Center for Climate Systems Modeling (C2SM) at ETH Zurich. The ECHAM-HAM simulations were performed using the ARCHER UK National Supercomputing Service. D. Watson-Parris receives funding from the European Union's Horizon 2020 research and innovation program iMIRACLI under Marie Skłodowska-Curie grant agreement No 860100 and also gratefully acknowledges funding from the NERC ACRIUSE project NE/S005390/1.

Data Availability Statement

Simulation data used in this manuscript is available at <http://doi.org/10.5281/zenodo.4282766>.

References

Albrecht, B. A. (1989). Aerosols, cloud microphysics and fractional cloudiness. *Science*, *245*(4923), 1227–1230.

Bellouin, N., Quaas, J., Gryspeerdt, E., Kinne, S., Stier, P., et al. (2020). Bounding global aerosol radiative forcing of climate change. *Reviews of Geophysics*, *58*(1), 8755–1209. <https://doi.org/10.1029/2019RG000660>

Danabasoglu, G., Lamarque, J.-F., Bacmeister, J., Bailey, D. A., DuVivier, A. K., Edwards, J., et al. (2020). The community earth system model version 2 (CESM2). *Journal of Advances in Modeling Earth Systems*, *12*(2), 1–99. <https://doi.org/10.1029/2019MS001916>

Diamond, M. S., & Wood, R. (2020). Limited regional aerosol and cloud microphysical changes despite unprecedented decline in nitrogen oxide pollution during the February 2020 COVID-19 shutdown in China. *Geophysical Research Letters*, *47*(17), e2020GL088913. <https://doi.org/10.1029/2020GL088913>

Forster, P. M., Forster, H. I., Evans, M. J., Gidden, M. J., Jones, C. D., Keller, C. A., et al. (2020). Current and future global climate impacts resulting from COVID-19. *Nature Climate Change*, *10*(10), 1–7. <https://doi.org/10.1038/s41558-020-0883-0>

Gettelman, A., Bardeen, C. G., McCluskey, C. S., Järvinen, E., Stith, J., Bretherton, C., et al. (2020). Simulating observations of Southern Ocean clouds and implications for climate. *Journal of Geophysical Research: Atmospheres*, *125*(21), e2020JD032619. <https://doi.org/10.1029/2020JD032619>

Gettelman, A., Hannay, C., Bacmeister, J. T., Neale, R. B., Pendergrass, A. G., Danabasoglu, G., et al. (2019). High climate sensitivity in the community earth system model version 2 (CESM2). *Geophysical Research Letters*, *46*(14), 8329–8337. <https://doi.org/10.1029/2019GL083978>

- Gettelman, A., & Morrison, H. (2015). Advanced two-moment bulk microphysics for global models. Part I: Off-line tests and comparison with other schemes. *Journal of Climate*, *28*(3), 1268–1287. <https://doi.org/10.1175/JCLI-D-14-00102.1>
- Goldberg, D. L., Anenberg, S. C., Griffin, D., McLinden, C. A., Lu, Z., & Streets, D. G. (2020). Disentangling the impact of the COVID-19 lockdowns on urban NO₂ from natural variability. *Geophysical Research Letters*, *47*(17), e2020GL089269. <https://doi.org/10.1029/2020GL089269>
- Hersbach, H., Bell, B., Berrisford, P., Hirahara, S., Horányi, A., Muñoz-Sabater, J., et al. (2020). The ERA5 global reanalysis. *Quarterly Journal of the Royal Meteorological Society*, *146*(730), 1999–2049. <https://doi.org/10.1002/qj.3803>
- IEA. (2020). *Global energy review 2020*, Paris, France: IEA. <https://www.iea.org/reports/global-energy-review-2020>
- Le Quéré, C., Jackson, R. B., Jones, M. W., Smith, A. J. P., Abernethy, S., Andrew, R. M., et al. (2020). Temporary reduction in daily global CO₂ emissions during the COVID-19 forced confinement. *Nature Climate Change*, *10*, 647–653. <https://doi.org/10.1038/s41558-020-0797-x>
- Le, T., Wang, Y., Liu, L., Yang, J., Yung, Y. L., Li, G., & Seinfeld, J. H. (2020). Unexpected air pollution with marked emission reductions during the COVID-19 outbreak in China. *Science*, *369*(6504), 702–706. <https://doi.org/10.1126/science.abb7431>
- Lian, X., Huang, J., Huang, R., Liu, C., Wang, L., & Zhang, T. (2020). Impact of city lockdown on the air quality of COVID-19-hit of Wuhan city. *The Science of the Total Environment*, *742*(10), 140556. <https://doi.org/10.1016/j.scitotenv.2020.140556>
- Liu, X., Ma, P.-L., Wang, H., Tilmes, S., Singh, B., Easter, R. C., et al. (2016). Description and evaluation of a new four-mode version of the modal aerosol module (MAM4) within version 5.3 of the community atmosphere model. *Geoscientific Model Development*, *9*(2), 505–522. <https://doi.org/10.5194/gmd-9-505-2016>
- Lohmann, U., & Neubauer, D. (2018). The importance of mixed-phase and ice clouds for climate sensitivity in the global aerosol–climate model ECHAM6-HAM2. *Atmospheric Chemistry and Physics*, *18*(12), 8807–8828. <https://doi.org/10.5194/acp-18-8807-2018>
- Molod, A., Takacs, L., Suarez, M., & Bacmeister, J. (2015). Development of the GEOS-5 atmospheric general circulation model: Evolution from MERRA to MERRA2. *Geoscientific Model Development*, *8*(5), 1339–1356. <https://doi.org/10.5194/gmd-8-1339-2015>
- Neubauer, D., Ferrachat, S., Siegenthaler-Le Drian, C., Stier, P., Partridge, D. G., Tegen, I., et al. (2019). The global aerosol–climate model ECHAM6.3–HAM2.3–Part 2: Cloud evaluation, aerosol radiative forcing, and climate sensitivity. *Geoscientific Model Development*, *12*(8), 3609–3639. <https://doi.org/10.5194/gmd-12-3609-2019>
- Sicard, P., De Marco, A., Agathokleous, E., Feng, Z., Xu, X., Paoletti, E., et al. (2020). Amplified ozone pollution in cities during the COVID-19 lockdown. *The Science of the Total Environment*, *735*, 139542. <https://doi.org/10.1016/j.scitotenv.2020.139542>
- Smith, C. J., Forster, P. M., Allen, M., Leach, N., Millar, R. J., Passerello, G. A., & Regayre, L. A. (2018). FAIR v1.3: A simple emissions-based impulse response and carbon cycle model. *Geoscientific Model Development*, *11*(6), 2273–2297. <https://doi.org/10.5194/gmd-11-2273-2018>
- Stevens, B., Giorgetta, M., Esch, M., Mauritsen, T., Crueger, T., Rast, S., et al. (2013). Atmospheric component of the MPI-M earth system model: ECHAM6. *Journal of Advances in Modeling Earth Systems*, *5*(2), 146–172. <https://doi.org/10.1002/jame.20015>
- Stier, P., Feichter, J., Kinne, S., Kloster, S., Vignati, E., Wilson, J., et al. (2005). The aerosol–climate model ECHAM5-HAM. *Atmospheric Chemistry and Physics*, *5*(4), 1125–1156. <https://doi.org/10.5194/acp-5-1125-2005>
- Twomey, S. (1977). The influence of pollution on the shortwave albedo of clouds. *Journal of the Atmospheric Sciences*, *34*(7), 1149–1152.
- Venter, Z. S., Aunan, K., Chowdhury, S., & Lelieveld, J. (2020). COVID-19 lockdowns cause global air pollution declines. *Proceedings of the National Academy of Sciences*, *117*(32), 18984–18990. <https://doi.org/10.1073/pnas.2006853117>
- Weber, J., Shin, Y. M., Sykes, J. S., Archer-Nicholls, S., Abraham, N. L., & Archibald, A. T. (2020). Minimal climate impacts from short-lived climate forcers following emission reductions related to the COVID-19 pandemic. *Geophysical Research Letters*, *47*(20), e2020GL090326. <https://doi.org/10.1029/2020GL090326>
- Wilks, D. S. (2006). On “field significance” and the false discovery rate. *Journal of Applied Meteorology and Climatology*, *45*(9), 1181–1189. <https://doi.org/10.1175/JAM2404.1>
- Yang, Y., Ren, L., Li, H., Wang, H., Wang, P., Chen, L., et al. (2020). Fast climate responses to aerosol emission reductions during the COVID-19 pandemic. *Geophysical Research Letters*, *47*(19), e2020GL089788. <https://doi.org/10.1029/2020GL089788>
- Zhang, K., O'Donnell, D., Kazil, J., Stier, P., Kinne, S., Lohmann, U., et al. (2012). The global aerosol–climate model ECHAM-HAM, version 2: Sensitivity to improvements in process representations. *Atmospheric Chemistry and Physics*, *12*(19), 8911–8949. <https://doi.org/10.5194/acp-12-8911-2012>
- Zhang, R., Zhang, Y., Lin, H., Feng, X., Fu, T.-M., & Wang, Y. (2020). NO_x emission reduction and recovery during COVID-19 in East China. *Atmosphere*, *11*(4), 433. <https://doi.org/10.3390/atmos11040433>